Impact of Substrate Temperature on Structural, electric and Optical characteristics of CuO Thin Films grown by JNS Pyrolysis Technique

Jhansi N
Government Arts College
Balasubramanian D (balad67@rediffmail.com)
Government Arts College
Jih-Hsing Chang
Chaoyang University of Technology
Mohanraj Kumar
Chaoyang University of Technology
Marnadu Raj
Sri Ramakrishna College of Arts and Science
Aslam Manthrammel M
King Khalid University
Mohd. Shkir
King Khalid University

Research Article

Keywords: JNS pyrolysis, monoclinic phase, CuO, thin film, electrical conductivity

Posted Date: August 3rd, 2021

DOI: https://doi.org/10.21203/rs.3.rs-767104/v1

Impact of Substrate Temperature on Structural, electric and Optical characteristics of CuO Thin Films grown by JNS Pyrolysis Technique

N. Jhansi[a], D. Balasubramanian[a], Jih-Hsing Chang[b], K. Mohanraj[b], R. Marnadu[c] M. Aslam Manthrammel[d], Mohd. Shkir[d]

[a]Raman Research Laboratory, PG & Research Department of Physics, Government Arts College, Tiruvannamalai-606603, Tamilnadu, India
[b]Department of Environmental Engineering and Management, Chaoyang University of Technology, Taichung 41349, Taiwan
[c]Department of Physics, Sri Ramakrishna Mission Vidyalaya College of Arts and Science, Coimbatore 20, Tamilnadu, India
[d]Advanced Functional Materials & Optoelectronics Laboratory, Department of Physics, College of Science, King Khalid University, Abha 61413, Saudi Arabia
**Corresponding author Phone No: +91 9443990556, E- Mail: balad67@rediffmail.com*

Abstract

JNS pyrolysis route has been successfully employed to grow CuO thin films at various substrate temperature, ranging from 300 to 600˚C. The XRD analyses revealed the monoclinic phased polycrystalline growth of the samples and exhibited the strong influence of the substrate temperature (ST) on the crystallite sizes. Optical transmission and bandgap studies also showed that sample bandgaps clearly rely upon the growth temperatures. The SEM micrographs displayed the agglomerated growth of particles having golf ball-like structures. The occurrence of Cu and O in the samples were confirmed through EDS analyses. The studies on DC electrical conductivities also shows strong dependency on the ST. A p-CuO/n-Si diode was fabricated at the ST of 600˚C and the diode parameters like barrier height (ϕ_b) and ideality factor (n) were determined under light and dark conditions.

Keywords: JNS pyrolysis; monoclinic phase; CuO; thin film; electrical conductivity.

1. Introduction

Transparent semiconducting oxide thin films are appealing because of their great optical qualities, high steadiness, and amazing electrical properties. Transparent conducting oxides (TCOs) delegated either n-type or p-type. As of late, exceptional consideration to investigate during the most recent couple of years has been concurred to TCOs of p-type semiconductors [1, 2], particularly copper oxide (CuO) is attributable owing to its various physiochemical properties that find wide scope of

utilization in gas sensor, optoelectronics, impetuses, field producers, optical switches, batteries, magneto resistance, solar cells, and high-temperature superconductors [3-10]. Moreover, CuO is a non-toxic eco-friendly chemical that attracts it as an alluring choice for many research applications, in all the oxide forms of the favored stage despite everything represents a test. They are found in two likely viz. CuO and Cu_2O of monoclinic (with bandgap, E_g of 1.3 - 2.1 eV) and cubic stages (with E_g of 2 - 2.6 eV) [11, 12].

Consequently, scientists have focused on the extension of strategies and working methodologies for changing particle morphologies of CuO which incorporate polyol, aqueous, sol-gel, warm oxidation, and so on. These reviews proposed the production of CuO powders made of nanoflowers [13], nanowires [14], nanoribbons [15], nanosheet [16], micro-rose [17], and nanobelts [18]. The CuO thin films can be grown by pulsed laser deposition [19], electrodeposition [20], CVD [21], sol-gel [22], successive ionic layer absorption and reaction method (SILAR) [23], solvothermal method [24], and thermal oxidations [25]. Among different technique, spray pyrolysis technique is simple, flexible, low-cost, and most versatile technique to coat the films directly on the substrate [26]. The method allows to tailor the film properties by precise optimization of numerous deposition parameters like substrate temperature, distance between nozzle and substrate, air pressure and spray rate, etc. Remarkably, crystallinity of grown thin film has strong dependency on the substrate temperature. In most cases, it would be the ST and annealing temperature that forms the basis of determining factor for the selectivity and the formation of the CuO or Cu_2O forms of the film. Hence in present investigation, we report growth of CuO thin films at various STs of 300-600 ˚C via the JNS pyrolysis route. The structural, morphological, optical and electric characterizations of the grown samples were carried out. Also, a p-CuO/n-Si diode was fabricated, and characteristic features were studied under dark and light environment.

2. Experimental details

2.1. CuO thin film preparation

CuO thin films were coated on glass substrates using JNS spray pyrolysis (fig 1a and b). Thoroughly cleaned glass substrates using meticulous procedures successively in double-distilled water, hydrochloric corrosive, sodium hydroxide,

isopropyl liquor respectively, and dried in RT were used for the deposition. 0.1 M of aqueous copper chloride ($CuCl_2$, Sigma-Aldrich) solution prepared in double-distilled water by stirring for an hour at RT was used as the precursor. The optimized conditions of CuO thin films are shown in Table 1. 5 ml of the precursor was taken each time for film deposition on the preheated-clean glass substrate (size: 2 X 2.5 cm) at four different STs from 300 to 600 ˚C.

2.2. p-CuO/n-Si diode fabrication

The CuO were grown on cleaned (100) n-Si wafer (size: 1x1 cm^2) using the JNSP setup to fabricate a p-CuO/n-Si junction diode. Initially, the n-Si wafer was cleaned artificially to keep away from the nearness of polluting influences. The piranha arrangement (H_2SO_4:H_2O_2 =3:1) was set up for taking out the polluting influences out of the wafer and diluted HF (HF: H_2O=1:10) was set up for expelling the native oxides on the Si surface, followed by rinsing in double-distilled water after each washing procedure before finally placing it on the substrate holder of JNSP arrangement [26, 27]. The 0.1 M copper chloride solution was sprayed on the n-Si wafer at 600 ˚C. The metal contacts from Si wafer and CuO film were extended using silver paste (from ELTECK Corporation). The developed device was allowed to dry at ambient temperature for 5 hours. The fabricated p-CuO/n-Si diode schematic structure is shown in Fig 2.

3. Materials characterization

The structural characteristics of the prepared film was studied by using a Bruker AXs D8 diffractometer XRD with CuKα1 wavelength of 1.5406 Å. The average crystallite sizes of the samples were calculated using well known Scherrer formula. The surface morphological studies of the films were carried out using a JEOL JEM 2100 scanning electron microscope and presence of elemental occurrences were analyzed by QUANTA FEG 250 EDX. The optical properties were studied by Perkin Elmer Lamda 35 UV-Vis spectrophotometer in the rage 300-900 nm. The DC electric conductivity and diode measurements of the p-CuO/n-Si films were probed using a Keithley Electrometer 6517-B.

4. Results and discussion

4.1 Structural analysis

Fig. 3(a-d) shows the XRD patterns of the CuO with various substrate temperatures. The monoclinic crystal structure was confirmed by an observed XRD patterns which is well suited with the standard JCPDS card (80-1916). The crystal plans (-111), (111), (112), (020), (-113) and (113) correspond to diffraction angles are 35.48˚, 38.70˚, 51.34˚, 53.42˚, 61.52˚ and 67.82˚ respectively. The peak intensities are found increasing with increasing ST which in turn affect the growth of (111) plane as is clearly shown Fig 3 (a-d). The average crystalline sizes are estimated using Scherrer formula,

$$D = \frac{0.9\times\lambda}{\beta\times cos\theta} \qquad (1)$$

Where λ is the X-ray wavelength (1.5421Å), β is the FWHM and θ is the diffraction angle. The estimated average crystallite size are of CuO are of the order of 87-78nm. The crystalline size decreases with increasing the substrate temperature which is revealed in Fig 4. The decrease particle size with temperature leads to the lattice expansion which is sensible by thermo dynamical view which is due to surface curvature, surface stress and surface defect. It was found that the temperature plays the role of increasing the crystalline property of the sample. The thicknesses of the films are measured using a stylus profilometer, and it was observed that the thickness decreases with increasing substrate temperature.

4.2. Morphology studies

Fig 5(a-c)- 8(a-c) display the morphological analyses of CuO films at different substrate temperatures ponders through the scanning electron micrographs. SEM micrographs confirm the influence of the ST in the morphologies of the grown films. It can be seen that very fine particles without distinct boundaries are formed at low STs. The CuO film grown at 300˚C exhibit irregular golf ball arrangement with inconsistent growth. When the ST is raised to 400˚C, number of golf balls with a distinct boundary increased with simultaneous reduction in the crystallite sizes. On increasing the substrate temperature, the improvement in fine structure of golf ball arrangement with size, shape and arrangement were noticed. However, when the temperature of the substrate increases the particle size decreases with regular shape and distinct grain boundaries, which satisfies the required conditions for the high-

quality thin films. Nevertheless, the CuO film deposited at 600°C possessed highest quality of the films.

4.3. Elemental analysis

EDS analysis have been used to identify the presence elements in sample (300˚C and 600˚C). The recorded EDS spectra are displayed in Fig9 (a-b), confirming the occurrences of Cu and O. The measured weight percentage (Wt%) values are shown in the corresponding spectrum. There is no evidence for the existence of other impurities in the CuO thin film samples.

4.4. Optical studies

The optical studies of CuO thin films were carried out using UV–Vis spectrophotometer at wavelength 400-900 nm. The recorded UV-Vis spectra are shown in Fig 10. It is evident from the figure that the transmittance is changing with substrate temperature. The observed high transparency value at 500˚C and 600˚C are due to less scattering and decreases in irregularity in the grain size [28]. At the substrate temperature of 600˚C, the film is highly transparent in the visible spectrum which makes it the very suitable material for the window in the solar cell. The energy band gaps of CuO films are obtained from the Tauc relation [29].

$$(\alpha h\upsilon)^n = B(h\upsilon - \mathrm{E_g}) \qquad (2)$$

where α– absorption coefficient, hν- energy of photon, $\mathrm{E_g}$- energy bandgap, B-constant and n- a number which describes the type of transition involved (2 for direct and ½ for indirect transitions). The bandgap energies corresponding to the direct allowed transitions are determined from the extrapolation of the linear segment of the plot to the X-axis. The band gap values of 300˚C, 400˚C, 500˚C and 600˚C CuO thin films are found as 2.9, 2.4, 2.1, and 1.8 eV, respectively. The existence of single slope suggests that the films have direct allowed transitions. The increase of substrate temperature in the CuO films caused the reduction of bandgap values as depicted in Fig 11.

4.5. DC conductivity

The investigation of electrical conductivities (σ) of CuO thin film (300 - 600˚C) were examined utilizing a Keithley electrometer 6517 B 2-probe arrangement.

The measurements are carried out in the 1- 10V range by monitoring the flow of current (I) into the film against the applied voltage (V), at measurement temperatures from 50˚C to 130˚C for the CuO films (300˚C- 600˚C) as demonstrated in fig. 12(a) - (d). The values of σ were obtained using the formula.

$$\sigma = \left(\frac{I}{V}\right) X \left(\frac{d}{A}\right) S/cm \qquad (3)$$

Where, d and A are the inter probe spacing and area of cross-section of the films, respectively. The film conductivities are found increasing with the temperature for consistent voltages as appeared in fig 10(a–d). The corresponding calculated average conductivities for 300, 400, 500 and 600 ˚C CuO thin films are $1.21X10^{-11}$, $7.21X10^{-10}$, $3.91X10^{-10}$ and $3.94X10^{-10}$ (S/cm), respectively (Fig.13). These results clearly demonstrate the σ values of CuO films are well enhanced with the increase in ST.

4.6. I-V characteristics of p-CuO/n-Si photodiode

I-V characteristics provides a detailed information about the fabricated devices such as diode nature/type, performance, and device quality and conduction mechanism. I-V characteristic studies of the p-CuO/n-Si junction diode was analyzed in the voltage ranging between is +4 to -4 V as shown in Fig. 14a. The current values of the diode was assessed under dark and light conditions to explore the photodiode performance, using a PEC-L01solar simulator. The diode measured under light (100 mW/cm^2) exposed condition showed a higher forward current than that of dark, suggesting the photo-conducting nature of the CuO/Si diode [30]. The maximum photocurrent of $4.5 X 10^{-5}$ A was recorded at 4 V. The conduction mechanism of the diode current can be explained by thermionic emission theory as described as shown [31-33].

$$I = I_0 \left[\exp\left(\frac{qV}{nK_BT}\right) - 1\right] \qquad (4)$$

where I_0 is the reverse saturation current given by

$$I_0 = AA^*T^2 \exp\left(-\frac{q\Phi_B}{K_BT}\right) \qquad (5)$$

where, n is ideality factor, Φ_B is the effective barrier height and A* is the Richardson constant while q, V, k_b, A and T are having their usual meaning. The calculated values of I_o are $1.74 X 10^{-04}$ (under dark) and $1.95 X 10^{-04}$ (under light) respectively. The parameter I_o mainly due to the diffusion of charge carrier from one side to other.

The values of n and Φ_B for the p-CuO/n-Si diode were obtained from semi-logarithmic plot (Fig. 14b) by the following equations [33,34].

$$n = \frac{q}{k_B T}\left(\frac{d(V)}{d(\ln(I))}\right) \quad (6)$$

$$\Phi_B = \frac{K_B T}{q} \ln\left(\frac{AA^* T^2}{I_0}\right) \quad (7)$$

The factors n and Φ_B are tabulated in Table 2 which are found to be varied from 19.15 -12.77 and 0.659-0.676 eV with dark and light. Compared to dark, the diode illuminated with light achieved a lower value of n and higher Φ_B. The deviated n value from unity could be owing to the existence of a thin interfacial layer at the p-CuO and n-Si interface, image force lowering, weak photo-carrier generation and carrier tunneling [35-39]. To study the photo-detector performance of the current device, we calculated many parameters related to the photo-detector including photosensitivity (P_S), responsivity (R), current gain (G), specific detectivity (D*) and quantum efficiency (EQE) using the relations.

$$P_s\,(\%) = \frac{I_{Ph} - I_D}{I_D} \times 100 \quad (8)$$

$$R = \frac{I_{Ph}}{PA} \quad (9)$$

$$G = \frac{I_{Ph}}{I_D} \quad (10)$$

$$D^* = \frac{R}{(2qI_D)^{1/2}} \quad (11)$$

$$EQE = \frac{Rhc}{q\lambda} \quad (12)$$

Where I_{Ph} and I_D are the photocurrent and the dark current, and P is the irradiation of the lamp. Other parameters like A, h, c, q and λ have their usual meaning. The measured photosensitivity of the p-CuO/n-Si photodiode was improved up to 288.32 %. Besides, The R, EQE and D* values of the diode are found to increase gradually with applied forward potential which was demonstrated in Fig. 15. This results implies the present diode is superiorly sensitive with forward voltage. The p-CuO/n-Si diode achieved a higher value of R=28.42 mA/cm^2, EQE=11.022 % and D*=1.467 X 10^{10} Jones at 4 V respectively. The generation of large photo-carrier with lesser recombination and more separation could be the reason for the obtained higher values [30,35,36]. The fabricated photodiode is highly acceptable for the fabrication of p-n photodetector.

5. Conclusion

CuO thin films were coated on glass substrates at various STs ranging from 300 to 600˚C through the JNS pyrolysis route. The XRD results depicted the polycrystalline nature with monoclinic structure. The estimated crystallite sizes (87-78nm) are found decreasing with increase in ST. The morphology analysis exhibited golf ball structures having randomized orientation of surface features, particularly for the CuO film grown at higher substrate temperatures. The EDX examination confirmed the presence of Cu and O in the films. From UV study, the bandgap of CuO films reduced from 2.9 to 1.8 eV as the substrate temperature increased. The electrical studies revealed that the conductivity values are highly dependent on substrate temperature. In summary, various results indicate that JNS pyrolysis technique is a low-cost and fast method for fabricating CuO thin films. The fabricated p-CuO/n-Si photodiode characteristics was studied under dark and light environments. Accordingly, the p-CuO/n-Si diode has a good photoconductive response and can be a prospective choice for photodetector applications.

Acknowledgement

The authors would like to express their gratitude to the Deanship of Scientific Research at King Khalid University, Abha, Saudi Arabia, for funding this work through Research Groups Program under Grant No. RGP-1/249/42.

Conflicts of interest

The authors declare they have no conflicts of interest.

Author contributions

All authors contributing equally.

Data availability statement

The data that support the findings of this study are already available inside the article.

Ethics approval and consent to participate

Not applicable

Consent for publication

Not applicable

References

[1] Z. Wang, P.K. Nayak, J.A. Caraveo-Frescas, H.N. Alshareef, Adv. Mater. 28 (2016) 3831–3892.

[2] E. Fortunato, P. Barquinha, R. Martins, Adv. Mater. 24 (2012) 2945–2986.

[3] W.Y. Ching, Y.-N. Xu, K. W. Wong, Ground state and optical properties of Cu_2O and CuO crystals, Phys.Rev.B: Condens. Matter 40 (1989) 7684–7695.

[4] L. C. Olsen, F. W. Addis, W. Miller, Experimental and theoretical studies of Cu_2O solar cells, Sol. Cells 7 (1983) 247–279.

[5] I˙. Y. Erdo˘gan, Ö. Güllü, Optical and structural properties of CuO nano-film:its diode application, J.Alloys Compd.492 (2010) 378–383.

[6] D. Gopalakrishna, K. Vijayalakshmi, C. Ravidhas, Effect of annealing on the properties of nanostructured CuO thin films for enhanced ethanol sensitivity, Ceram.Int. 39 (2013)7685–7691.

[7] D. Zappa, E. Comini, R. Zamani, J. Arbiol, J. R. Morante, G. Sberveglieri, Preparation of copper oxide nanowire-based conductometric chemical sensors, Sens.Actuators, B: Chem.182 (2013) 7–15.

[8] W. Zhang, S. Ding, Z. Yang, A. Liu, Y. Qian, S. Tang, etal., Growth of novel nano-Structured copper oxide (CuO) films on copper foil, J. Cryst. Growth 291 (2006)479–484.

[9] A. Fullana, S. S. Sidhu, Fate of PAHs in the post-combustion zone:partial oxidation of PAHs to dibenzofuran over CuO, J.Anal.Appl.Pyrolysis 74 (2005) 479–485.

[10] M. -F. Dignac, N. Pechot, M. Thevenot, C. Lapierre, H. Bahri, G. Bardoux, etal., Isolation of soillignins by combination of ball-milling and cellulolysis: evaluation of purity and isolation efficiency with pyrolysis/GC/MS, J.Anal.Appl.Pyrolysis 85 (2009) 426–430.

[11] E. M. Alkoy, P.J. Kelly, Vacuum 79 (2005) 221–230.

[12] T. Maruyama, Copper oxide thin films prepared by chemical vapor deposition from copper dipivaloylmethanate, Sol. Energy Mater. Sol. Cells 56 (1998) 85–92.

[13] Y. Wang, T. Jiang, D. Meng, J. Yang, Y. Li, Q. Ma, J. Han, Appl. Surf. Sci. 317 (2014) 414.

[14] C.J. Love, J.D. Smith, Y.H. Cui, K.K. Varanasi, Nanoscale 3 (2011) 4972.

[15] B. Liu, H.C. Zeng, J. Am. Chem. Soc. 126 (2004) 8124.

[16] Y. Li, S. Chang, X. Liu, J. Huang, J. Yin, G. Wang, D. Cao, Electrochim. Acta 85 (2012) 393.

[17] D.P. Dubal, G.S. Gund, R. Holze, C.D. Lokhande, J. Power Sources 242 (2013) 687.

[18] J.Y. Xiang, J.P. Tu, L. Zhang, Y. Zhou, X.L. Wang, S.J. Shi, J. Power Sources 195 (2010) 313.

[19] A.P. Chen, H. Long, X.C. Li, Y.H. Li, G. Yang, P.X. Lu, Controlled growth and characteristics of single-phase Cu2O and CuO films by pulsed laser deposition, Vacuum83 (2009) 927–930.

[20] R.P. Wijesundera, Fabrication of the CuO/Cu2O heterojunction using an electrodeposition technique for solar cell applications, Semicond. Sci. Technol. 25(2010) 045015.

[21] T. Koh, E. O'Hara, M.J. Gordon, Growth of nanostructured CuO thin films viamicroplasma-assisted, reactive chemical vapor deposition at high pressures, J.Cryst. Growth. 363 (2013) 69–75.

[22] H.W. Qin, Z.L. Zhang, X. Liu, Y.J. Zhang, J.F. Hu, Room-temperature ferromagnetism in CuO sol-gel powders and films, J. Magn. Magn. Mater. 322 (2010)1994–1998.

[23] K. Mageshwari, R. Sathyamoorthy, Physical properties of nanocrystalline CuOthin films prepared by the SILAR method, Mater. Sci. Semicond. Process. 16(2013) 337–343.

[24] W. Zhang, S. Ding, Z. Yang, A. Liu, Y. Qian, S. Tang, S. Yang, Growth of novelnanostructured copper oxide (CuO) films on copper foil, J. Cryst. Growth 291(2006) 479–484.

[25] C.H. Xu, C.H. Woo, S.Q. Shi, Formation of CuO nanowires on Cu foil, Chem. Phys.Lett. 399 (2004) 62–66.

[26] K. Mohanraj, D. Balasubramanian, J. Chandrasekaran, Synthesis and characterization of Ruthenium-doped CdO nanoparticle and its n-RuCdO/p-Si junction diode application, J. Alloys Compd.779 (2019) 762-775.

[27] K. Mohanraj, D. Balasubramanian, J. Chandrasekaran, A. Chandra Bose, Synthesis and characterizations of Ag-doped CdO nanoparticles for P-N junction diode application, Mater. Sci. Semicond. Process. 79 (2018) 74-91.

[28] S. S. Roy, A. H Bhuiyan, J. Podder Optical and Electrical Properties of Copper Oxide Thin Films Synthesized by Spray Pyrolysis Technique, sensors &Transducers, 191 (2015) 21- 27.

[29] J. Tauc, Optical properties and electronic structure of amorphous Ge and Si, Mater. Res. Bull. 3 (1968) 37–46.

[30] R. Marnadu, J. Chandrasekaran, S. Maruthamuthu, P. Vivek, E. Vijayakumar, Superior photoresponse MIS Schottky barrier diodes with honeycomb:Sn-WO_3 films for ultraviolet photodetector application, New Journal of Chemistry, 44 (2020) 7708-7718.

[31] A. Tataroglu, S. Altındal, The distribution of barrier heights in MIS type Schottky diodes from current–voltage–temperature (I–V–T) measurements, Journal of Alloys and Compounds 479, (2009) 893–897

[32] O. Pakma, N. Serin, T. Serin, and Ş. Altındal, The double Gaussian distribution of barrier heights in Al/TiO_2/p-Si (metalinsulator-semiconductor) structures at low temperatures, J. Appl. Phys. 104 (2008) 014501

[33] M. Ozer, D.E. Yıldız, S. Altındal, M.M. Bulbu, Temperature dependence of characteristic parameters of the Au/SnO_2/n-Si (MIS) Schottky diodes, Solid-State Electronics. 51 (2007) 941–949

[34] S. Altındal, H. Kanbur, D.E. Yıldız, M. Parlak, Current conduction mechanism in Al/p-Si Schottky barrier diodes with native insulator layer at low temperatures, Applied Surface Science, 253 (2007) 5056–5061

[35] R. Marnadu, J. Chandrasekaran, M. Raja, M. Balaji, S. Maruthamuthu, P. Balraju, Influence of metal work function and incorporation of Sr atom on WO_3 thin films for MIS and MIM structured SBDs, Superlattices and Microstructures. 119 (2018) 134–149.

[36] R. Marnadu, J. Chandrasekaran, M. Raja, M. Balaji, V. Balasubramani, Impact of Zr content on multiphase zirconium–tungsten oxide (Zr–WO_x) films and its MIS structure of Cu/Zr–WOx/p-Si Schottky barrier diodes,

Journal of Materials Science: Materials in Electronic. 29 (2018) 2618–2627.

[37] A. Karabulut, I .Orak, A. Türü, Electrical characteristics of Au/Ti/HfO_2/n-GaAs metal-insulator-semiconductor structures with high-k interfacial layer, International Journal of Chemistry and Technology. 2 (2018) 116 – 122.

[38] A. Karabulut, I. Orak, M. Caglar, and A. Turut, The Current–Voltage Characteristics Over The Measurement Temperature Of 60–400 K In The Au/Ti/n-GaAs Contacts With High Dielectric HfO_2 Interfacial Layer, Surface Review and Letters. 26 (2019) 1950045.

[39] A. Karabulut, H. Efeoglu, and A. Turut, Influence of Al_2O_3 barrier on the interfacial electronic structure of Au/Ti/n-GaAs structures, Journal of Semiconductors. 38 (2017) 054003.

Figures

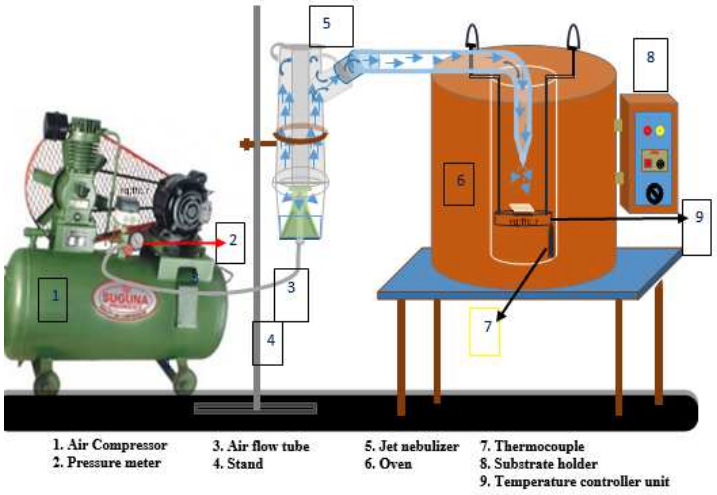

Fig. 1a. Schematic illustration of jet nebulizer spray pyrolysis (JNSP) system

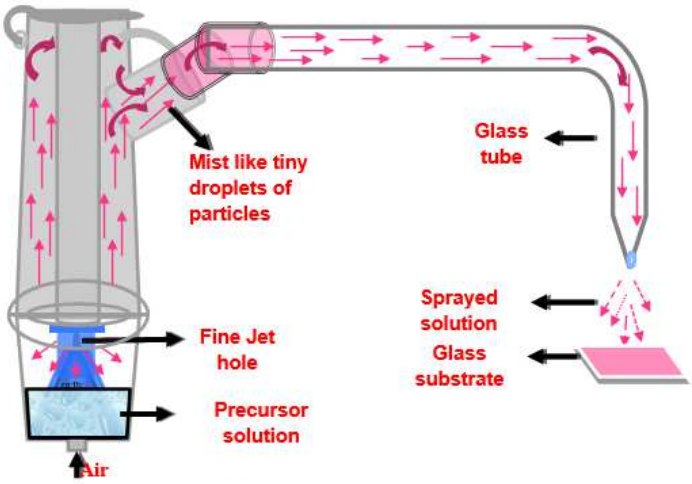

Fig. 1b. Schematic drawing of jet nebulizer

Figure 1

See image above for figure legend.

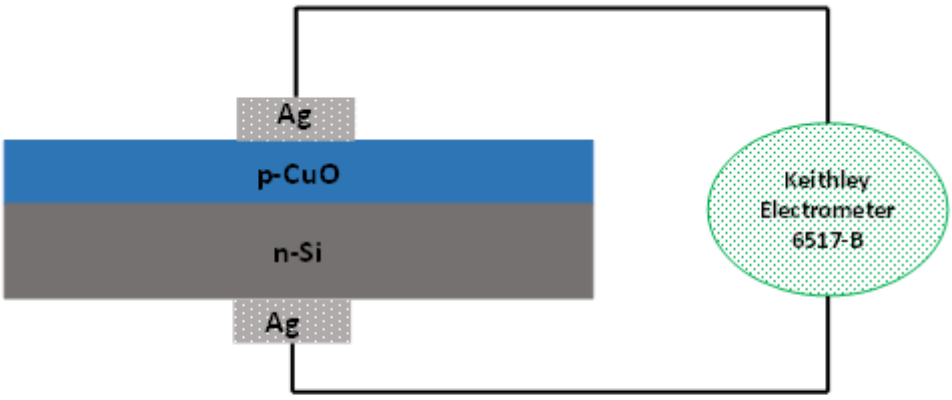

Fig. 2. The schematic structure of p-CuO/n-Si diode.

Figure 2

See image above for figure legend.

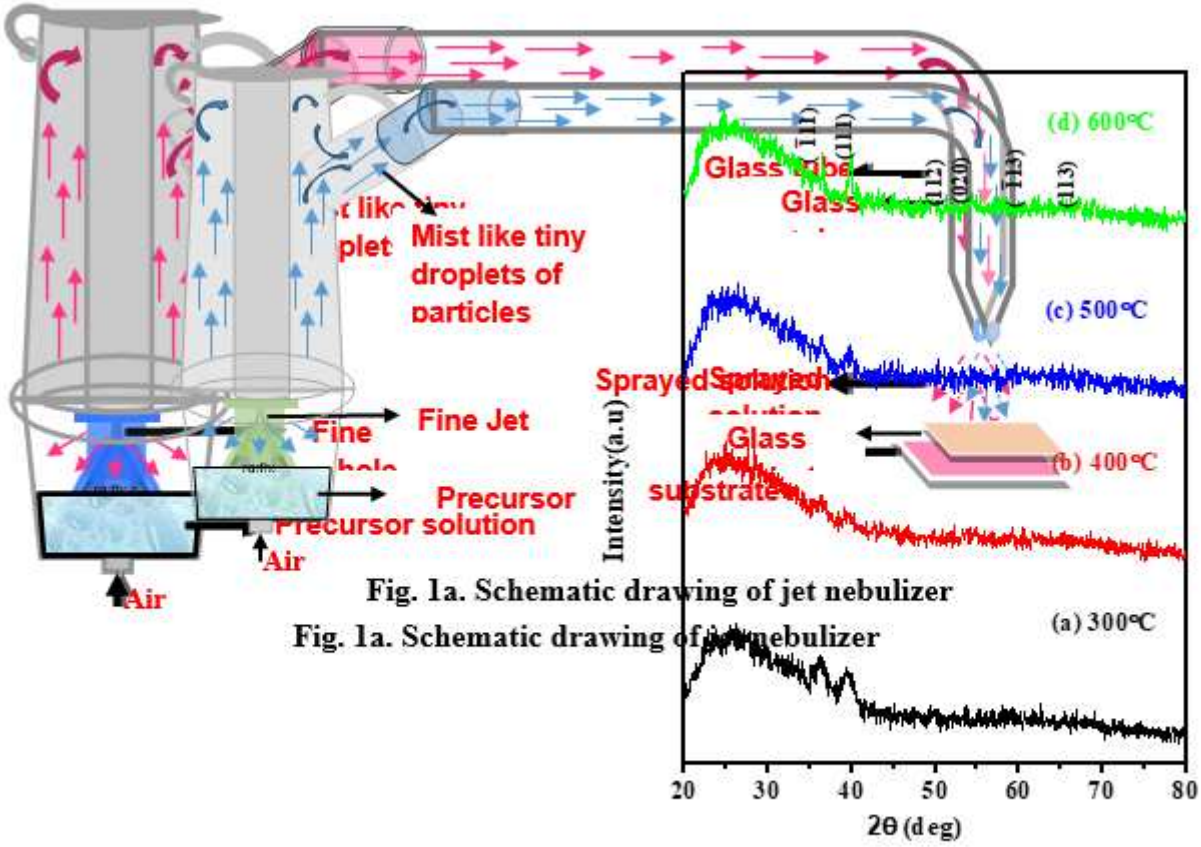

Fig. 1a. Schematic drawing of jet nebulizer

Fig. 1a. Schematic drawing of jet nebulizer

Fig. 3. X-ray Diffraction patterns of CuO thin films.

Figure 3

See image above for figure legend.

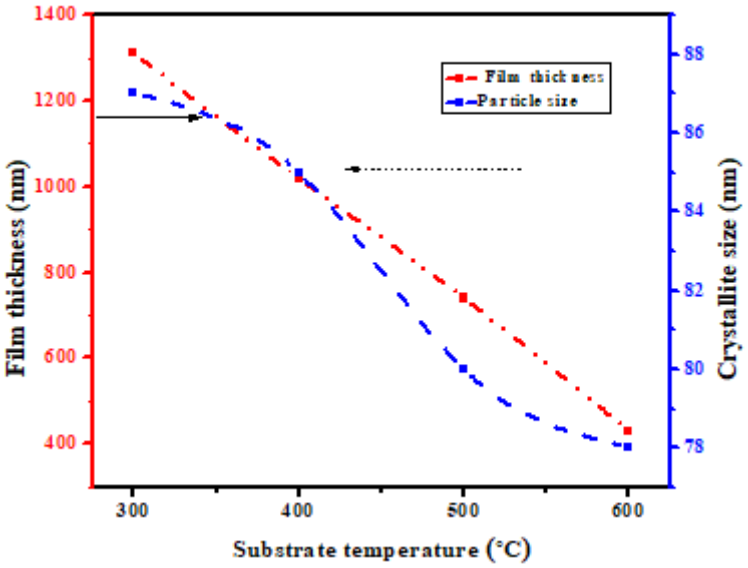

Figure 4

Variation of particle size and film thickness with substrate temperature.

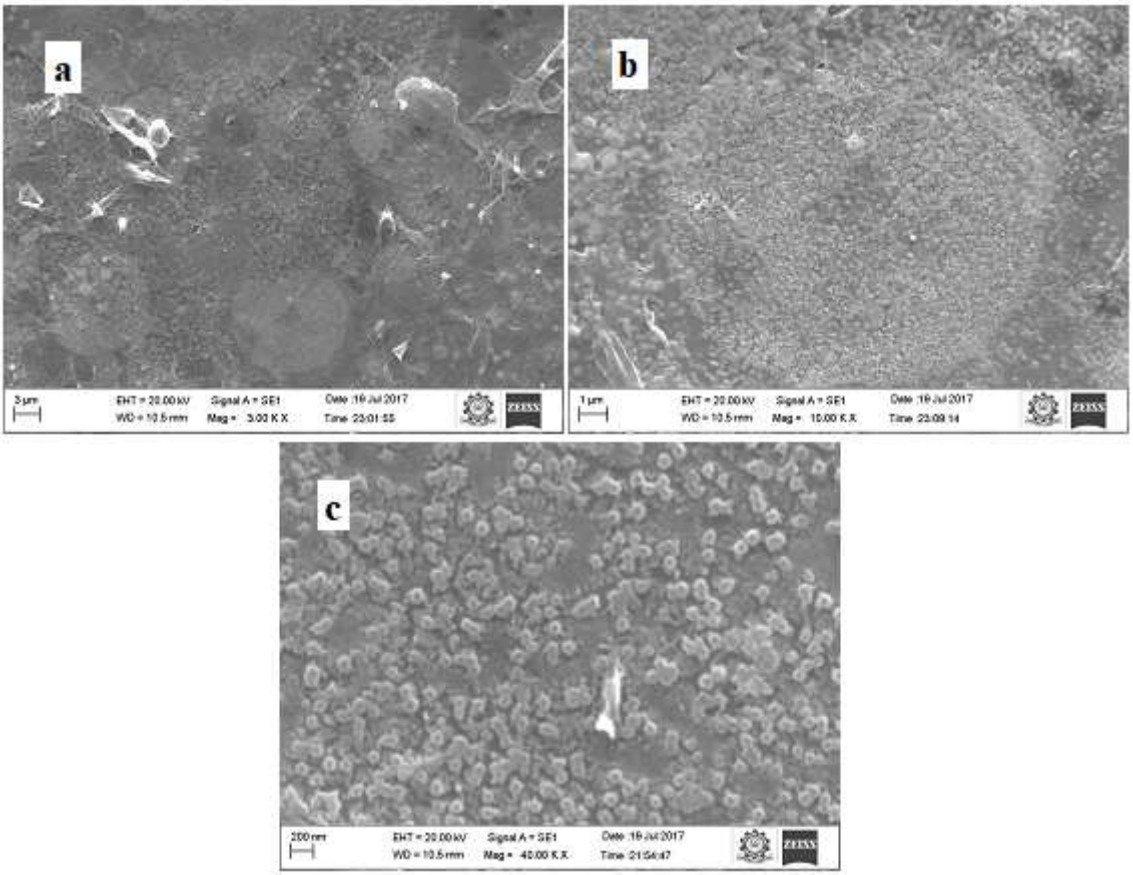

Figure 5

(a-c) Scanning electron microscope images of CuO thin films at 300˚C substrate temperature

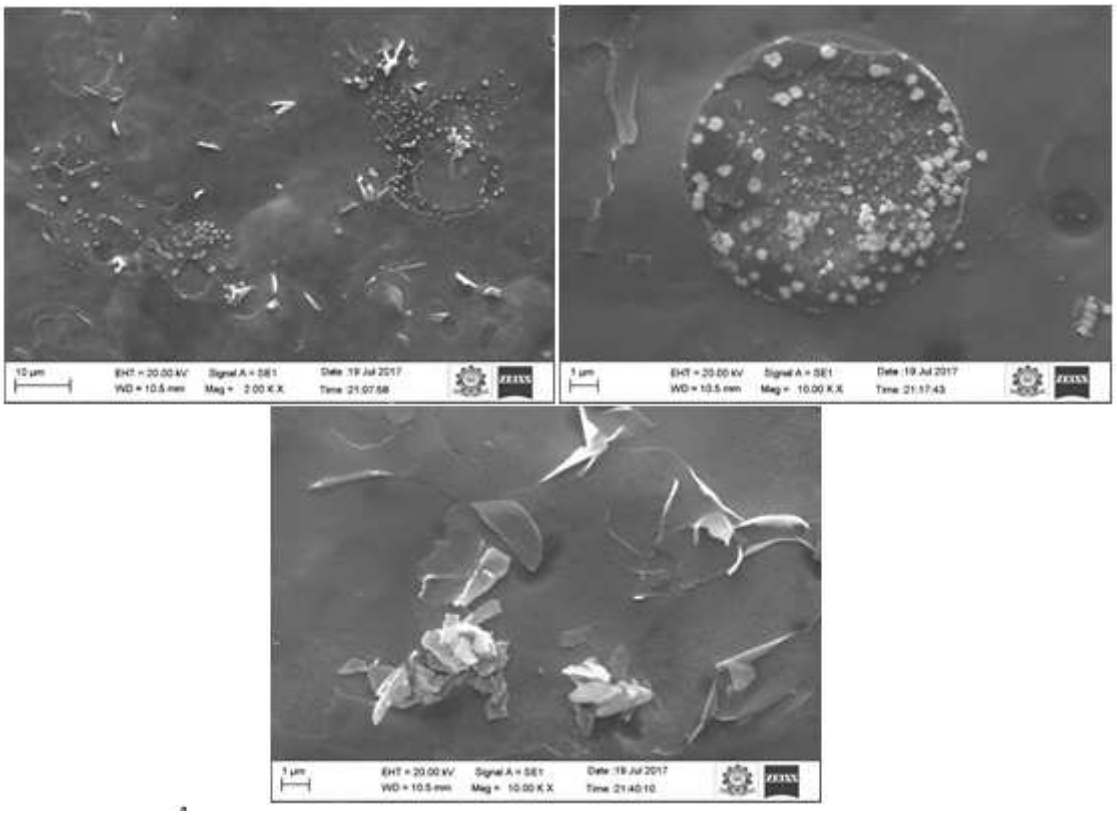

Figure 6

(a-c). Scanning electron microscope images of CuO thin films at 400˚C substrate temperature.

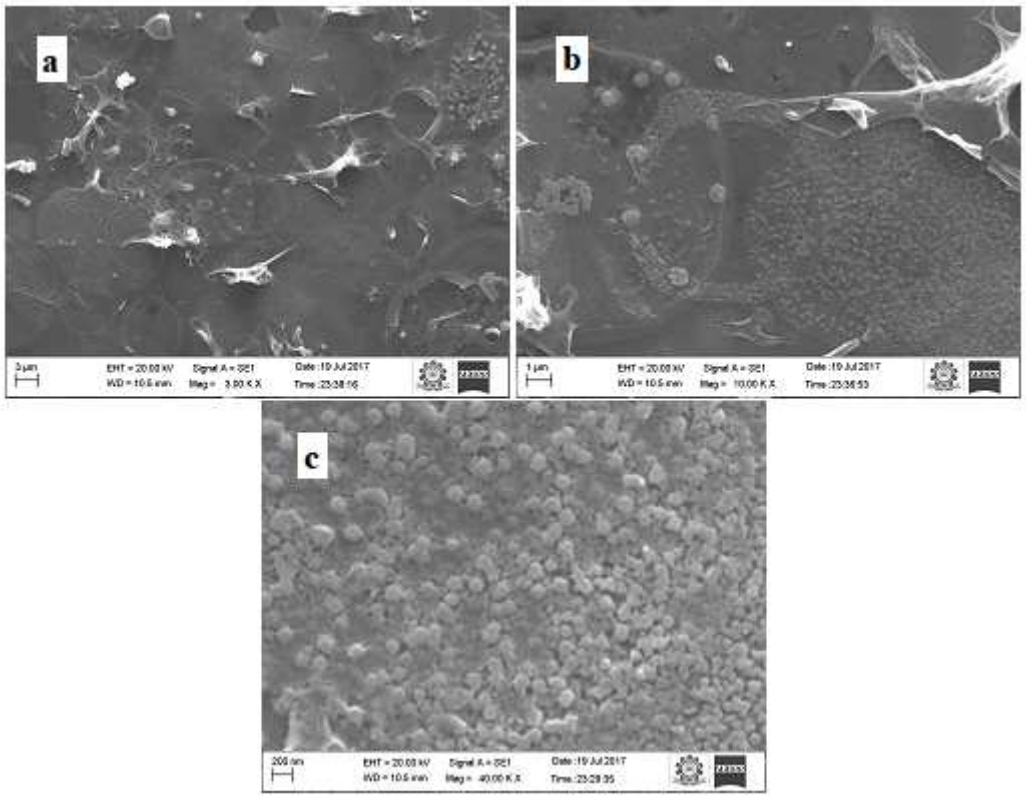

Figure 7

(a-c). Scanning electron microscope images of CuO thin films at 500˚C substrate temperature.

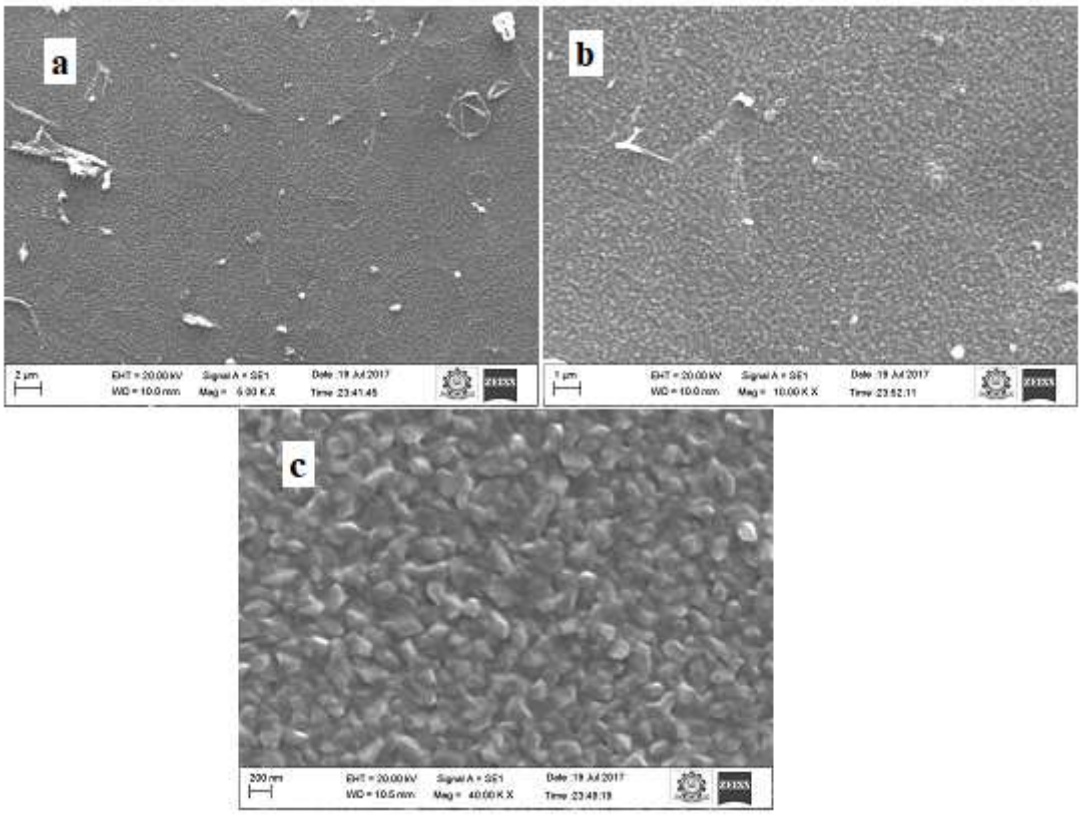

Figure 8

(a-c). Scanning electron microscope images of CuO thin films at 300˚C substrate temperature.

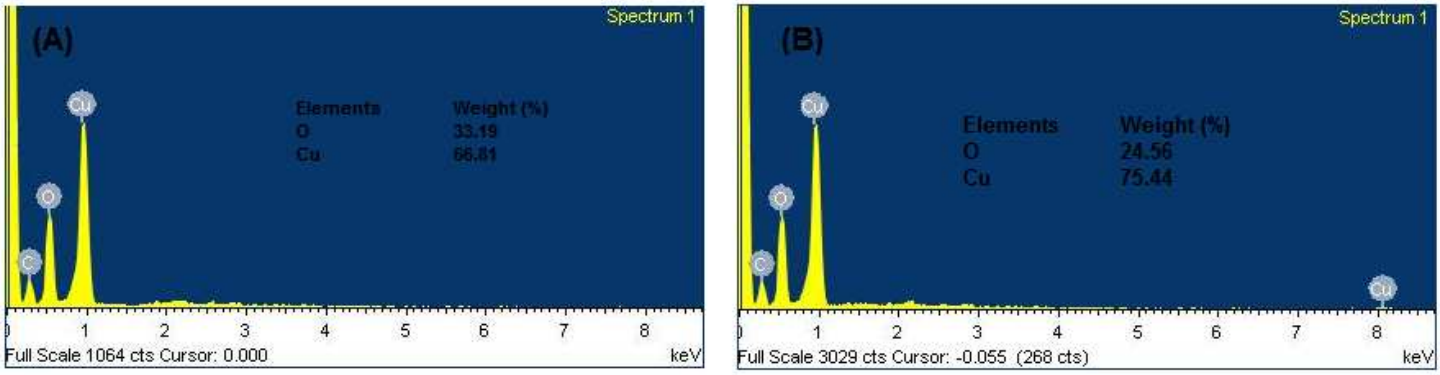

Figure 9

EDS Spectra of CuO thin films at (a) 300˚C and (b) 600˚C.

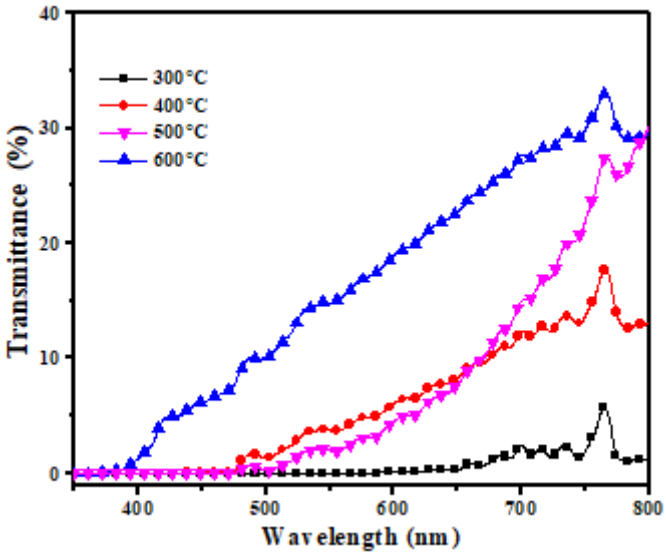

Figure 10

Transmittance spectra of CuO thin films.

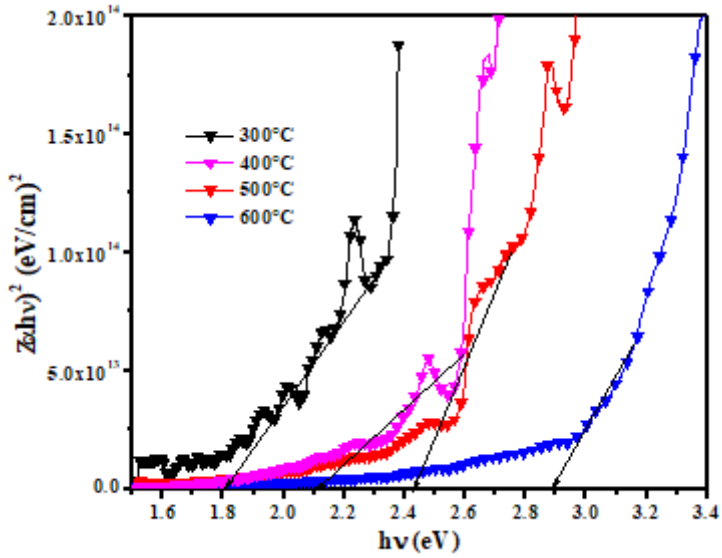

Figure 11

Plot of (αhν)2Vs hν for CuO thin films.

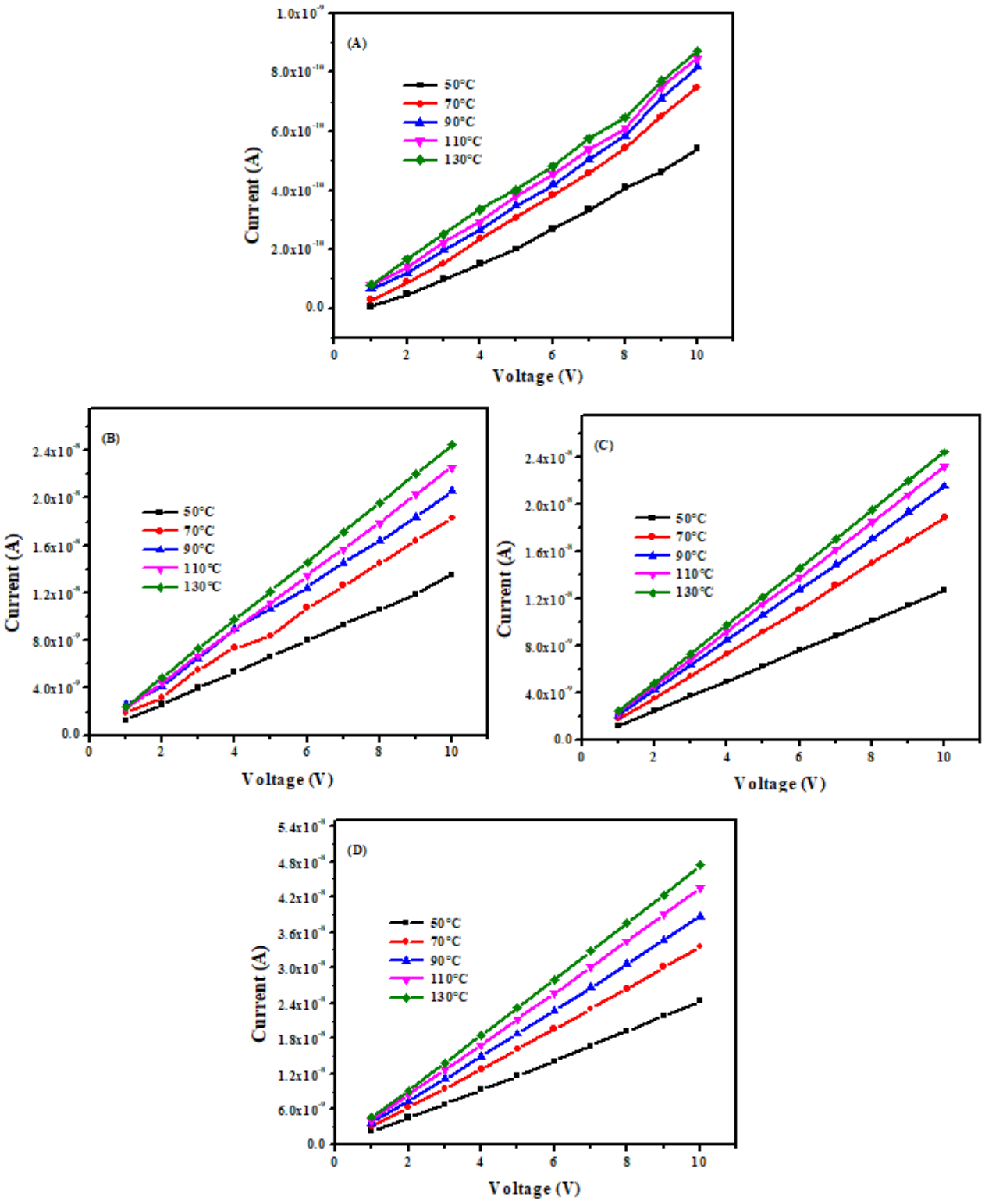

Figure 12

The conductivity of CuO thin films at (A) 300˚C(B) 400˚C (C) 500˚C (D) 600˚C

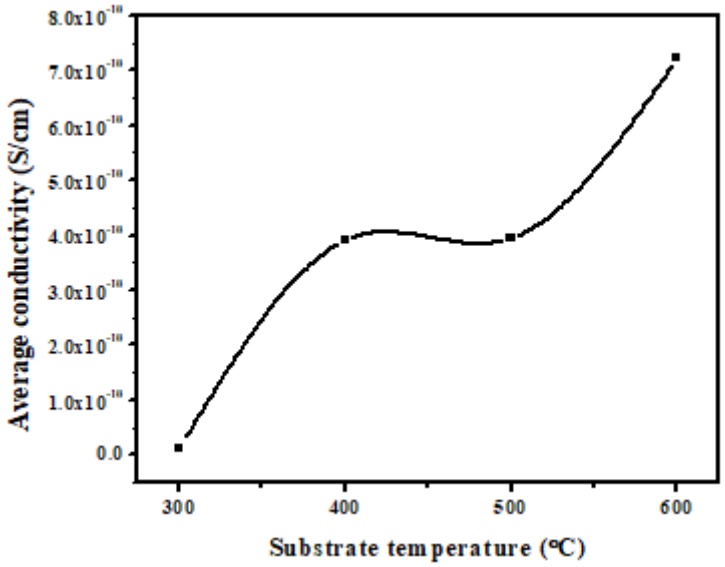

Figure 13

The average conductivity of CuO thin film.

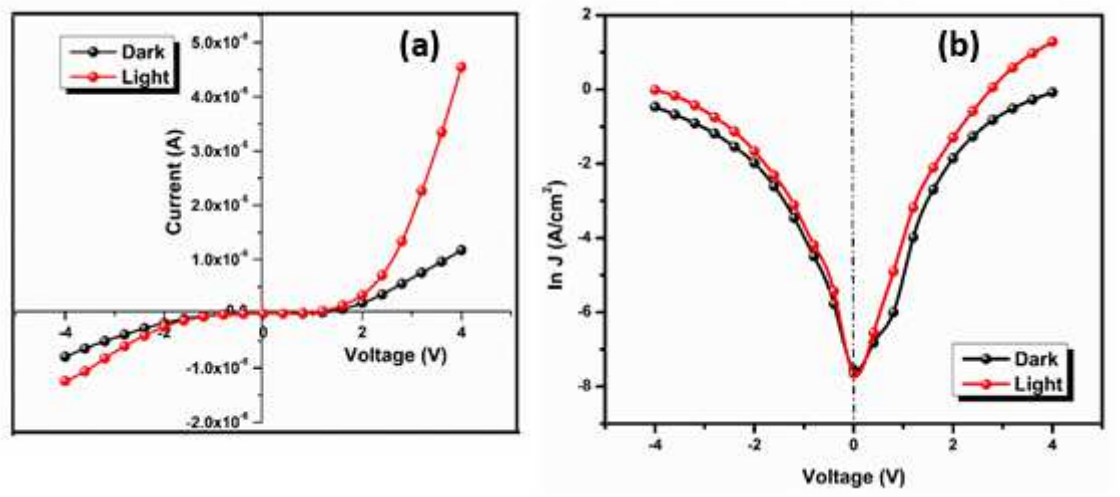

Figure 14

(a) I-V characteristics and (b) semi-logarithmic plot of the p-CuO/n-Si junction diode.

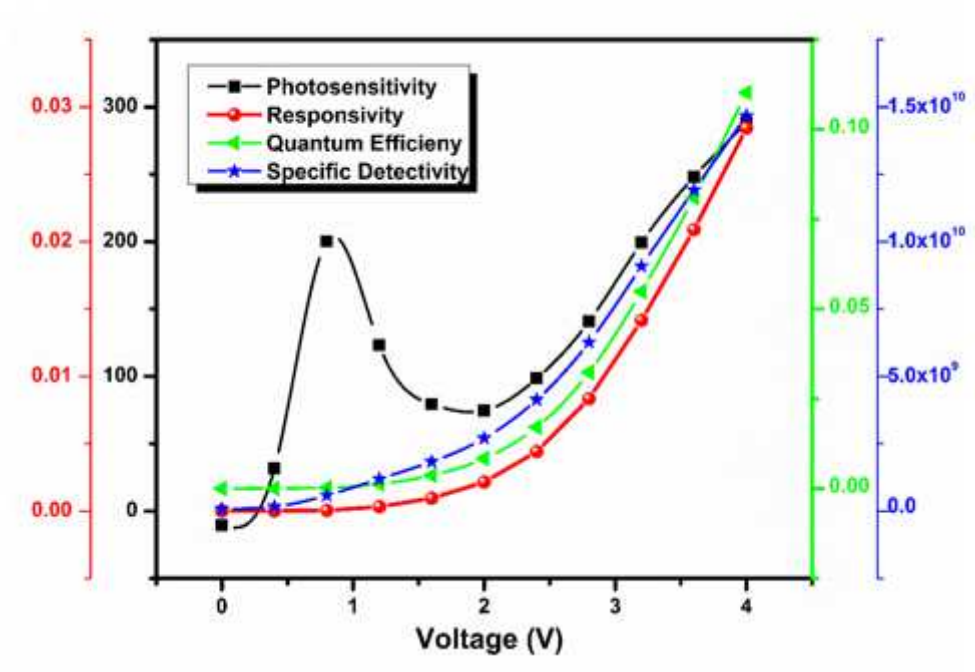

Figure 15

Variations of photo-detector parameters with applied voltage